Structure of exotic nuclei and superheavy elements in a relativistic shell model

M. Rashdan
Department of Mathematics and Theoretical Physics, Atomic Energy Authority, P.O. 13759, Cairo, Egypt
(Received 17 May 2000; published 2 March 2001)

We have carried out a study of the structure of heavy exotic nuclei and superheavy elements in the framework of the relativistic mean field (RMF) theory, adopting a new relativistic force, (NL-RA1). Pairing correlations, are treated in the Bardeen-Cooper-Schrieffer formalism with a constant gap approximation, adopting a new model for the energy gap, where a Gaussian shape distribution depending on the particle numbers is assumed. This pairing model is found to successfully describe heavy open shell nuclei. The new relativistic force NL-RA1 successfully reproduced the ground state properties of finite nuclei as well as nuclear matter. This force is used to study the structure of Sn and Pb isotopic chains, while considering extreme values of isospin. It is found that the binding energies, neutron and proton rms radii, and neutron skins are fairly described. Furthermore, the charge rms radii, and the anomalous kind in the isotopic shifts of the charge radii of the Pb isotopic chain are also well described by the NL-RA1 force. In comparison with other relativistic forces like, TM1, NL-SH, and NL1 it is found that the TM1 force could describe the binding energy, while it overestimates the charge radii of Pb isotopes. The NL-SH produced larger binding in the lighter side of ^{208}Pb and smaller charge radii. The NL1 force shows systematic discrepancies in both the binding energies as well as the charge radii, due to their larger symmetry energies. Other relativistic forces, like NL-Z and NL-Z2, have also been tested and found to largely overestimate the charge radii of Pb isotopes. We also investigated the ground state properties of superheavy elements in the region $Z \geqslant 98$ and it is found that the NL-RA1 force fairly described the binding energy. The element $^{298}_{184}114$ is predicted to be the next spherically doubly magic superheavy nucleus to ^{208}Pb, where a large stable two-proton gap for the $Z=114$ proton shell on the order of 3 MeV, depending on the effective interaction and pairing model, has been predicted. We also found strong evidence of other spherically doubly magic superheavy elements, such as the element $^{292}_{172}120$.

DOI: 10.1103/PhysRevC.63.044303 PACS number(s): 21.60.Cs, 24.10.Jv

I. INTRODUCTION

The study of exotic nuclei is one of the main frontiers of nuclear structure research [1–5]. It can provide more basic data, now for increasingly unstable systems, that will help in answering the open questions in the nuclear structure theory, ranging from the understanding of the interaction between nucleons in the nuclear medium and its relationship to the underlying fundamental interactions to the understanding of the many-body manifestations of the nucleus as a system of correlated fermions. A prominent example is the better understanding of shell structure reached by seeing how closures can develop as proton and neutron numbers change. Investigations at the limits of existence, at and even beyond the drip lines, have developed a new completely unforeseen structure. They present interesting problems in themselves and lead to a deeper comprehension of the nucleus in general.

For nuclei far from stability a very interesting aspect is an increase of their radial dimension with decreasing particle separation energies [6–10]. Extreme cases are halo nuclei, loosely bound few-body system, and the existence of neutron skins. These skins change the nuclear properties, such as the rapid increasing in the nuclear radii, and on the other hand can provide an opportunity for studying the behavior of abnormal nuclear matter with very large isospin. This could be helpful in improving the reliability of calculations of neutron star properties. The weak binding and corresponding looseness of the particle continuum, together with the need for the explicit treatment of few-body dynamics, makes the theoretical study of these subjects both extremely interesting and difficult [2]. A better theory for nuclear many-body systems should handle the new phenomena of exotic nuclei as well as of superheavy elements.

The study of superheavy elements has been a hot topic for the last two decades. Evidence of several new elements with the atomic numbers $Z=109-112$ [11–13], the new isotopes ^{265}106, ^{266}106, ^{273}110 [14–17], and, more recently, the element ^{293}118 and several of its α-decay daughter nuclei [18] have added to the momentum of the activity in the pursuit of the superheavy nuclei [19–25]. These discoveries were certainly the outstanding highlights at the top of the periodic table, and on the other hand, have clearly demonstrated the existence of shell-stabilized nuclei.

An interesting theoretical approach that recently proved to be very powerful for an effective microscopic description of nuclear systems is the relativistic mean-field (RMF) theory [26–48]. The RMF theory explicitly includes mesonic degrees of freedom and describes the nucleons as Dirac particles. Nucleons interact in a relativistic covariant manner through the exchange of the isoscalar scalar self-coupling σ meson, the isoscalar vector ω meson, the isovector-vector ρ meson, and the photon. The model is based on the one-boson exchange description of the nucleon-nucleon interaction. The RMF theory has the advantage that, with the proper relativistic kinematics and with the mesons and their properties already known or fixed from the properties of nuclear matter and of a small number of known nuclei, the method gives excellent results for the binding energies, root mean square (rms) radii, quadrupole and hexadecapole deformations, and other nuclear properties of nuclei. The role of relativity in the short-ranged region of nuclear force and its effect in produc-

ing saturation at the correct density and binding energy in nuclear matter is now being recognized [49]. Another major attractive feature of the RMF approach is that the spin-orbit interaction and the associated nuclear shell structure comes out naturally as arising from meson-nucleon interactions. The inclusion of the ρ meson takes care of the neutron proton asymmetry. Recently, the pseudospin symmetry of the nuclear shell model has been understood as a relativistic symmetry [38].

The RMF theory has been used by many authors to study stable, unstable, and superheavy nuclei [6,21–48], employing different RMF forces. However, various usually employed RMF forces, which give a fair description of normal stable nuclei, give quite different predictions for unstable nuclei [39] and superheavy elements [22–25]. For example, Greiner and collaborators [22–24] perform detailed comparisons of various RMF parametrizations (as well as various nonrelativistic Skyrme parametrizations) for the superheavy nuclei. They found that total energies are less well reproduced and the forces show different isotopic and isotonic trends, even for the known superheavies [22,23]. Furthermore, shell closures, deformations, and stability have been found to depend strongly on the parametrization. A similar conclusion has been obtained in [25] when investigating the new element 118 and several of its alpha-decay daughter nuclei, through various RMF forces.

In this work we study exotic nuclei and superheavy elements in the framework of the RMF theory, adopting a new relativistic force. Pairing correlations are treated through the Bardeen-Copper-Schrieffer (BCS) formalism by introducing a new model for the energy gap. This paper is organized as follows. Section II presents a summary of the RMF approach with results of our new force for nuclear matter and closed shell nuclei in comparison with different RMF forces. In Sec. III pairing correlations are discussed in detail. Numerical calculations of the ground state properties of Sn and Pb isotopic chains are presented and discussed in Sec. IV, with a comparison of the available experimental data as well as with various RMF forces. The predictions for superheavy elements are presented and discussed in Secs. V and VI with a comparison of other theoretical predictions. Finally, Sec. VII presents a summary and conclusion.

II. THEORY

The Lagrangian density for Dirac nucleons interacting with the scalar self-coupling σ-meson field Φ, the self-coupling neutral vector ω-meson field $\mathbf{V}^{\mu}(\mu=0,1,2,3)$, the isovector-vector ρ-meson field $\vec{\rho}^{\mu}$, and the electromagnetic fields A^{μ}, is written as [22–48]

$$
\begin{aligned}
L=&\overline{\psi}_i(\gamma^{\mu}i\partial_{\mu}-M)\psi_i+\frac{1}{2}\partial^{\mu}\Phi\partial_{\mu}\Phi-\frac{1}{2}m_{\sigma}^2\Phi^2-\frac{1}{3}b_2\Phi^3\\
&-\frac{1}{4}b_3\Phi^4-g_s\overline{\psi}_i\psi_i\Phi-\frac{1}{4}\Omega^{\mu\nu}\Omega_{\mu\nu}+\frac{1}{2}m_{\omega}^2\mathbf{V}^{\mu}\mathbf{V}_{\mu}\\
&+\frac{1}{4}c_3(\mathbf{V}^{\mu}\mathbf{V}_{\mu})^2-g_{\omega}\overline{\psi}_i\gamma^{\mu}\psi_i\mathbf{V}_{\mu}-\frac{1}{4}\vec{\mathbf{B}}^{\mu\nu}\vec{\mathbf{B}}_{\mu\nu}+\frac{1}{2}m_{\rho}^2\vec{\rho}^{\mu}\vec{\rho}_{\mu}\\
&-g_{\rho}\overline{\psi}_i\gamma^{\mu}\vec{\tau}\psi_i\vec{\rho}_{\mu}-\frac{1}{4}\mathbf{F}^{\mu\nu}\mathbf{F}_{\mu\nu}-e\overline{\psi}_i\gamma^{\mu}\frac{1+\tau_{3i}}{2}\psi_i\mathbf{A}_{\mu}. \quad (1)
\end{aligned}
$$

Vectors in isospin space are denoted by arrows. The Dirac spinor ψ_i represents the nucleon with mass M. m_{σ}, m_{ω}, and m_{ρ} are the masses of the σ meson, the ω meson, and the ρ meson, respectively. The meson-nucleon coupling constants, g_{σ}, g_{ω}, and g_{ρ}, and the meson masses are parameters adjusted to fit nuclear matter data and some static properties of finite nuclei. $\Omega^{\mu\nu}$,$\vec{\mathbf{B}}^{\mu\nu}$, and $F^{\mu\nu}$ are field tensors [26–36]. τ_3 is the third component of the isospin.

To describe the ground-state properties of finite nuclei we need a static solution of the above Lagrangian. For this case the meson and electromagnetic fields are time independent, whereas the nucleon wave functions oscillate with the single-particle energy ϵ_i. Further due to time-reversal symmetry the vector (spatial) parts of the vector and electromagnetic potentials vanish. The charge conservation implies that only the third component of the isovector-vector field ρ_0 contributes to the interaction with nucleons. Under these conditions variation of the action integral give the following Euler-Lagrange field equations for the nucleon, meson, and photon fields

$$
\begin{aligned}
&\left[-i\vec{\boldsymbol{\alpha}}\cdot\vec{\boldsymbol{\nabla}}+\beta M(r)^*+g_{\omega}V_0(r)+g_{\rho}\tau_3\rho_0(r)+e\frac{1+\tau_3}{2}A_0(r)\right]\\
&\quad\times\psi_i(r)=\epsilon_i\psi_i(r), \quad (2)
\end{aligned}
$$

$$
\begin{aligned}
&\frac{d^2\Phi_0(r)}{dr^2}+\frac{2}{r}\frac{d\Phi_0(r)}{dr}-m_{\sigma}^2\Phi_0(r)\\
&\quad=g_s\rho_s(r)+b_2\Phi_0^2(r)+b_3\Phi_0^3(r), \quad (3)
\end{aligned}
$$

$$
\frac{d^2V_0(r)}{dr^2}+\frac{2}{r}\frac{dV_0(r)}{dr}-m_{\omega}^2V_0(r)=-g_{\omega}\rho_v(r)+c_3V_0^3(r), \quad (4)
$$

$$
\frac{d^2\rho_0(r)}{dr^2}+\frac{2}{r}\frac{d\rho_0(r)}{dr}-m_{\rho}^2\rho_0(r)=-g_{\rho}\rho_{\rho}(r), \quad (5)
$$

$$
\frac{d^2A_0(r)}{dr^2}+\frac{2}{r}\frac{dA_0(r)}{dr}=-e\rho_c(r). \quad (6)
$$

We have neglected the contribution of antiparticles. $M(r)^*(=M+g_s\Phi_0(r))$ is the effective mass of the nucleon.

The Lorentz scalar, baryonic, isovector, and charge densities, ρ_s,ρ,ρ_{ρ}, and ρ_c are given by

$$
\rho_s(r)=\sum_{i=1}^{\Gamma}n_i\overline{\psi}_i(r)\psi_i(r), \quad (7)
$$

$$
\rho(r)=\sum_{i=1}^{\Gamma}n_i\overline{\psi}_i(r)\gamma^0\psi_i(r), \quad (8)
$$

$$
\rho_{\rho}(r)=\sum_{i=1}^{\Gamma}n_i\overline{\psi}_i(r)\gamma^0\tau_{3i}\psi_i(r), \quad (9)
$$

$$\rho_c(r)=\sum_{i=1}^{\Gamma} n_i \bar{\psi}_i(r)\gamma^0\frac{1+\tau_{3i}}{2}\psi_i(r), \tag{10}$$

where the occupation probability n_i is introduced to allow for a pairing treatment of open shell nuclei. The size of the valence space, Γ_p or Γ_n, is chosen to include all occupied states up to the magic shell just being opened; thus for magic nuclei there will be no pairing. The total binding energy of the system derived from the above RMF Lagrangian is given by [26–30]

$$E=E_{\rm part}+E_\sigma+E_\omega+E_\rho+E_c+E_{\rm pair}-E_{\rm c.m.}. \tag{11}$$

The $E_{\rm part}$ is the sum of the single-particle energies of the nucleons ϵ_i, weighted by the pairing probability n_i. E_σ, E_ω, E_ρ, E_c, and $E_{\rm pair}$ are the contributions of the meson fields σ, ω, and ρ, the Coulomb field, and pairing energy. The effect of pairing interaction has been added for open shell nuclei in the BCS formalism with a constant gap approximation. Pairing will be discussed in detail in the next section. The $E_{\rm c.m.}=\frac{3}{4}41A^{-1/3}$, is the nonrelativistic approximation for the center-of-mass energy.

The coupled field equations (2)–(10) are solved self-consistently employing different RMF forces. As discussed in Sec. I, most of the RMF parameter sets, which satisfactorily described stable nuclei, give different predictions for both exotic nuclei and superheavy elements. This could be due to the fact that the parameters of these different relativistic forces have been adjusted to reproduce some properties of stable nuclei and nuclear matter, which could be insufficient to determine a well definite RMF parameter set. Moreover, the compressibility K of nuclear matter, which is not determined well in experiment, increases the ambiguities in the determination of the RMF parameters.

It is worth mentioning that in [34], we have studied the ability of removing some of the ambiguities in the determination of the RMF parameter sets by deriving a RMF force, NL-RA, from Dirac-Brueckner-Hartree-Fock (DBHF) calculations of nuclear matter [49–53], which on the other hand, is a better account of nuclear correlations. However, this force could not describe unstable nuclei and superheavies better than some other RMF forces. In the DBHF calculations the two-body correlations are exactly included, by summing over all second-order ladder diagrams. However, other many-body effects such as three-body forces and the effect of quantum vacuum are important and should be explicitly included. Thus the determination of a unique realistic RMF parameter set is very difficult and tedious. At present, one could determine a good RMF parameter set by investigating most of the present sets in describing many different phenomena of nuclear systems. In fact, this is one of the main goals of studying nuclei far from stability as well as superheavy elements, where the isotopic properties of different nuclear forces can be tested. In [22–25] more investigations have been performed on various RMF parameter sets, such as NL1 [29,32], NL-Z [29,32], PL-40 [29], NL-SH [35], TM1 [37], and the two recent forces NL-Z2 [24] and NL-VT1 [24] (as well as nonrelativistic Skyrme parametrizations [24]), in describing finite nuclei and superheavy elements. Although, these forces have been found to describe the properties of finite nuclei within acceptable errors, there are significant differences between them which, as expected, greatly affected the predictions of superheavy elements. These differences can be summarized as follows. There are differences in surface properties. Most forces perform very well in that respect, but the forces NL-SH and TM1 produce a too small surface thickness and do not work as well in fission calculations. There are differences in the effective mass. The forces NL-Z, PL-40, and NL-Z2 have low effective mass, which is expected to affect the level density and shell structure for large systems [24]. There are differences in the equation of state. The forces NL-Z, PL-40 and the more recent ones NL-Z2 and NL-VT1 produce a very soft equation of state with too small incompressibility. For example, the PL-40 force has $K=166$ MeV, which is much smaller than the lowest value deduced from the experimental data (≈ 200 MeV). There are differences in the symmetry energy. The forces NL1, NL-Z, PL-40, NL-Z2, and NL-VT1 have much larger symmetry energy than the others. There are differences in describing the energy levels and all the relativistic forces have problems in describing single-particle energies below the Fermi energy as well, especially for larger systems [24]. There are differences in the spin-orbit splitting, although most of the RMF forces perform well in that respect. There are differences in the description of neutron rich nuclei as well as superheavy elements, which will be discussed in detail in the next sections.

In this work we introduce a new relativistic force, NL-RA1, which could better describe the isotopic properties of nuclei as well as most of the other nuclear properties. We also perform a detailed comparison between the predictions of different RMF parameter sets for nuclear matter, stable and unstable nuclei, as well as superheavy elements. In the determination of the new relativistic parameters NL-RA1 we fix the masses of the nucleon, ω meson, and ρ meson to their experimental values and fit the mass of the σ meson, which is not well determined from experiments, and the coupling constants in order to simultaneously reproduce the correct ground state properties of a wider range of finite nuclei as well as the saturation properties of nuclear matter. The obtained parameter set, NL-RA1, is listed in Table I, with its predictions for nuclear matter (see also Fig. 1). For comparison we presented in Table I and Fig. 1 results for NL1, NL-SH, and TM1 forces, which currently used in RMF models [22]. The results for the binding energies and charge rms radii as well as the single-particle energies of closed shell nuclei ranged from ^{16}O to ^{208}Pb, which are obtained by solving the relativistic mean field equations (1)–(11), employing the new NL-RA1 force, which are presented in Tables II and III. These tables present results for NL-SH and TM1 forces for comparison.

For the case of nuclear matter, Fig. 1 and Table I show that all forces give almost similar binding energy per particle and saturation density but they give different compressibilities. The NL1 gives a softer equation of state with $K=211.7$ MeV. The NL-RA1 and TM1 forces give equation of states with $K=285$ and 281 MeV, respectively. The value of K deduced from the breathing mode is about $K=210$

TABLE I. The new relativistic NL-RA1 parameter set with its predictions for nuclear matter in comparison with the NL-SH, NL1, and TM1 parameter sets [20].

Parameter	NL-RA1	NL-SH	NL1	TM1
M (MeV)	939	939	938	938
m_σ (MeV)	515.7	526.059	492.25	511.198
m_ω (MeV)	783	783	795.25	783
m_ρ (MeV)	763	763	763	770
g_σ	10.362 31	10.4436	10.138	10.0289
g_ω	12.921 154	12.945	13.285	12.6139
g_ρ	4.405 879 5	4.383	4.976	4.6322
$b2$ (fm^{-1})	−10.059 947	−6.909 91	−12.172	−7.2325
$b3$	−27.5565	−15.8337	−36.265	0.6183
$c3$	0	0	0	71.3075
M^*/M	0.6	0.6	0.57	0.634
a_{sym} (MeV)	36.1	36.1	43.6	36.9
K (MeV)	285	354.95	211.7	281
$\rho_0(\mathrm{fm}^{-3})$	0.1466	0.146	0.154	0.145
E/N (MeV)	16.15	16.4	16.328	16.3

± 30 MeV, while recent investigations [54] deduced larger values of $K \approx 300 \pm 30$ MeV. Thus both NL-RA1 and TM1 forces predicted the recent values of K, while NL1 predicted that of the breathing mode, which is smaller. The NL-SH gives a stiffer equation of state with larger compressibility, $K = 355$ MeV. Another major difference comes from the asymmetry parameter, which is important in describing the asymmetry prosperties of nuclear systems. The NL1 force produced a much larger value $a_{\mathrm{sym}} \approx 43$ MeV, and thus produces lager symmetry energies, while the other forces produced a reasonable value ≈ 36 MeV, which is closer to the empirical value ≈ 32 MeV.

One also notices that both the NL-RA1 and TM1 forces predict almost similar binding energy per nucleon up to nuclear matter densities less than and around 0.2 fm^{-3}, as seen from Fig. 1. For densities larger than 0.2 fm^{-3} the TM1

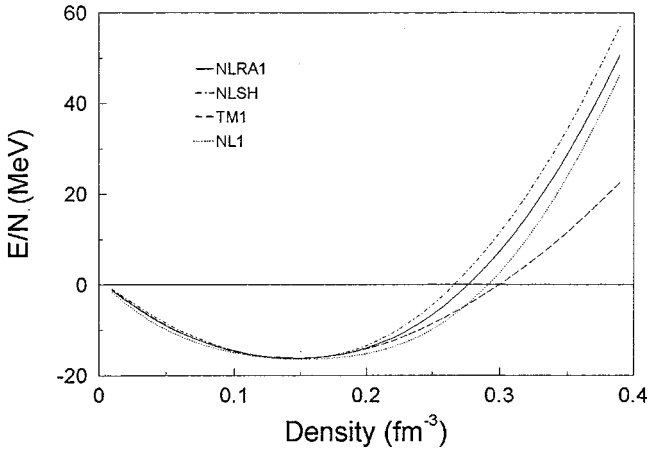

FIG. 1. The binding energy per nucleon in nuclear matter against nuclear matter density calculated by NL-RA1 force in comparison with NL-SH, NL1, and TM1 forces.

TABLE II. The binding energy per particle and charge radii of stable nuclei calculated, by solving the relativistic field equations [1–11], employing the relativistic NL-RA1 force in comparison with the NL-SH and TM1 forces and with experiments.

		NL-RA1	NL-SH	TM1	Expt.
^{16}O	E/A (MeV)	−8	−7.933	−8.06	−7.98
	r_{ch} (fm)	2.66	2.64	2.65	2.7±0.05
^{40}Ca	E/A (MeV)	−8.55	−8.5	−8.62	−8.55
	r_{ch} (fm)	3.44	3.46	3.43	3.45
^{48}Ca	E/A (MeV)	−8.67	−8.66	−8.666	−8.67
	r_{ch} (fm)	3.42	3.41	3.424	3.47
^{56}Ni	E/A (MeV)	−8.65	−8.66	−8.59	−8.64
	r_{ch} (fm)	3.7	3.7	3.73	3.75
^{100}Sn	E/A (MeV)	−8.3	−8.32	−8.3	−8.26
	r_{ch} (fm)	4.46	4.46	4.48	—
^{132}Sn	E/A (MeV)	−8.37	−8.39	−8.36	−8.36
	r_{ch} (fm)	4.69	4.68	4.71	—
^{208}Pb	E/A (MeV)	−7.87	−7.9	−7.88	−7.87
	r_{ch} (fm)	5.5	5.48	5.52	5.5

force predicted larger binding due to the self-interaction term of the ω-meson exchange. This is one of the main differences between the TM1 force and the other relativistic forces. This term, which on the other hand increases the parameters of the RMF model, gives more binding at higher

TABLE III. (a) Proton and (b) neutron single-particle energies and spin-orbit splittings calculated by NL-RA1 in comparison with NL-SH and TM1 forces and experimental values.

		NL-RA1	NL-SH	TM1	Expt.
		(a)			
^{16}O	$^1s_{1/2}$ (MeV)	−37.52	−37.86	−36.52	−40±8
	$^1p_{3/2}$ (MeV)	−18.08	−18.34	−17.73	−18.4
	$^1p_{1/2}$ (MeV)	−11.53	−11.6	−12.16	−12.1
	$\delta\epsilon_{\mathrm{s.o.}}$ (MeV)	6.55	6.74	5.57	6.3
^{40}Ca	$^1s_{1/2}$ (MeV)	−45.43	−45.33	−43.5	−50±8
	$^1p_{3/2}$ (MeV)	−30.32	−30.66	−29.44	−34±5
	$^1p_{1/2}$ (MeV)	−25.9	−26.35	−25.95	−34±6
	$^1d_{5/2}$ (MeV)	−15.57	−15.9	−15.18	−14±2
	$^2s_{1/2}$ (MeV)	−9.43	−8.83	−9.11	−10±1
	$^1d_{3/2}$ (MeV)	−8.87	−9.04	−9.5	−7±1
		(b)			
^{16}O	$^1s_{1/2}$ (MeV)	−41.72	−42.08	−40.7	−45.7
	$^1p_{3/2}$ (MeV)	−21.98	−22.3	−21.63	−21.8
	$^1p_{1/2}$ (MeV)	−15.4	−15.4	−16.01	−15.7
	$\delta\epsilon_{\mathrm{s.o.}}$ (MeV)	6.58	6.9	5.62	6.1
^{40}Ca	$^1s_{1/2}$ (MeV)	−53.58	−53.5	−51.6	−61.5
	$^1p_{3/2}$ (MeV)	−38.12	−38.5	−37.22	−61.5
	$^1p_{1/2}$ (MeV)	−33.71	−34.2	−33.74	−42.1
	$^1d_{5/2}$ (MeV)	−23.03	−23.4	−22.64	−23.6
	$^2s_{1/2}$ (MeV)	−16.8	−16.2	−16.45	−18.2
	$^1d_{3/2}$ (MeV)	−16.24	−16.48	−16.91	−15.6

densities. This is also seen in Table II, where larger bindings are obtained for ^{16}O (129 MeV) and ^{40}Ca (845 MeV), since these nuclei have relatively large central densities. In fact the TM1 force has been designed for nuclei with Z larger than 20, while for $Z \leqslant 20$ another parameter set, TM2, has been introduced [37], which presents some kind of discontinuity in the RMF parameters.

Tables II and III show that the binding energies, radii, and single-particle energies are well described by NL-RA1 force. The NL-SH gives lower binding for ^{40}Ca, while the TM1 force gives larger binding for ^{16}O and ^{40}Ca. These two forces give larger binding for ^{208}Pb. A slightly smaller charge radius for ^{208}Pb is predicted by the NL-SH force, while TM1 predicts a slightly larger radius. The results of the energy levels and spin-orbit splitting are also quite interesting. The NL-SH and TM1 forces predicted a wrong proton and neutron level ordering for ^{40}Ca, where the levels $^2s_{1/2}$ and $^1d_{3/2}$ are interchanged, while the NL-RA1 force predicts the correct level ordering, as seen from Table III(a) and (b). This table also shows that the NL-RA1 force better describes the spin-orbit splitting $\delta\epsilon_{\text{s.o.}}(=\,^1p_{1/2}-\,^1p_{3/2})$ in ^{16}O, where the relative errors, $|\delta\epsilon^{\text{cal}}_{\text{s.o.}}-\delta\epsilon^{\text{expt}}_{\text{s.o.}}|/\delta\epsilon^{\text{expt}}_{\text{s.o.}}$, in percent for NL-RA1, NL-SH, and TM1 are about 4, 7, and 12, respectively, for protons and 8, 13, and 8 for neutrons.

III. PAIRING CORRELATION

For open shell nuclei pairing correlations are usually treated by the BCS formalism or by a density dependent approach. For example, Ring and collaborators [29,41–46] treated pairing correlation self-consistency through the relativistic Hartree-Bogoliubov approach. In that approach a two-body force for pairing correlation, such as the phenomenological finite-range Gogny force [55], has been used.

In the present work pairing correlations are treated by the BCS formalism by introducing a new model for the energy gap. In the BCS formalism the occupation probability is given by

$$n_i=\frac{1}{2}\left[1+\frac{\epsilon_i-\lambda}{\sqrt{(\epsilon_i-\lambda)^2+\Delta^2}}\right], \tag{12}$$

where λ is the Fermi energy for neutrons or protons determined by imposing the condition

$$\sum_{i=1}^{\Gamma} n_i=N_n \quad \text{or} \quad N_p. \tag{13}$$

This pairing contributes a quantity to the energy

$$E_{\text{pair}}=-\Delta\sum_{i=1}^{\Gamma}\sqrt{n_i(1-n_i)}. \tag{14}$$

In the following we consider two approximations for the energy gap Δ. The first is the usual empirical average formula of Bohr and Mottelson [56]

$$\Delta_n=\Delta_p=\Delta=11.2/\sqrt{A} \quad \text{MeV}. \tag{15}$$

We denote this approximation for Δ by model I, or shortly, Δ I. One can also use the empirical mass difference formula for the energy gaps $\Delta_{n,p}$ [56] in order to describe odd and even proton or neutron numbers. However, the experimental masses are not available for most of drip-line nuclei, especially that with extreme values of isospin, as well as most of the superheavy elements. In this work we approximate $\Delta_{n,p}$ by the following Gaussian distribution model:

$$\Delta_{n,p}=\begin{cases}\alpha_{n,p}\,\exp-\left(\dfrac{N_c}{N_{n,p}}\right)^2 & \text{for} \quad N_{n,p}\leqslant N_c\,,\\ \alpha_{n,p}\,\exp-\left(\dfrac{N_n,p}{N_c}\right)^2 & \text{for} \quad N_{n,p}>N_c,\end{cases} \tag{16}$$

where

$$N_c=\tfrac{1}{2}(N_{c1}+N_{c2}). \tag{17}$$

N_{c1} and N_{c2} are taken to be the two nearest magic numbers of N_n or N_p, i.e., $N_{c1}<N_{n,p}<N_{c2}$. $\alpha_{n,p}$ is a strength scaling parameter which should, in principle, depend on the particle numbers as well as the effective interaction. In this work we consider, as an approximation, a constant value of this parameter $\alpha_p=\alpha_n=5$ (5.5) MeV for odd (even) neutron or proton numbers N_n or N_p. We denote this model of the energy gap by model II or shortly, Δ II.

Model II for the energy gap has been tested for open shell nuclei and it is found to better describe heavy nuclei. For example, for ^{238}U we get for the binding energy, employing the relativistic force NL-RA1, the value -1800.5 MeV, which is very close to the experimental binding -1801.7 MeV. Model I gives the value -1793 MeV. The corresponding values of the energy gap obtained from Eqs. (15) and (16) are $\Delta_p=\Delta_n=0.726$ MeV in model I and $\Delta_p=1.53$ MeV and $\Delta_n=1.65$ MeV in model II. For ^{90}Zr model I gives 783 MeV for the binding energy, while model II gives 784.6 MeV, which is closer to the experimental value $\sim$784 MeV. In this case Δ_p increases from 1.18 MeV in model I to 1.92 MeV in model II. The changes in the rms radii are found to be small, especially for stable nuclei. For example, for ^{238}U both the charge and proton radii are found to have very small changes and the neutron radius r_n is slightly increased from 6.056 fm in model I to 6.065 fm in model II. This slight change in the neutron radii increases the neutron skin, r_n-r_p, from 0.264 to 0.276 fm.

For pairing model II has also been tested for the available experimental binding for nuclei heavier than ^{238}U and it is found to well describe the binding energies. However, in order to better describe the separation energy for superheaviest, with $Z\geqslant 98$, the parameters N_{c1}, N_{c2}, and α_n are modified. For the case of protons with $N_p\geqslant 98$ we consider the values 82, 114, and 126 for N_{c1} and the corresponding values of N_{c2} are considered to be 126, 228, and 228, respectively. For neutrons N_{c1} is assumed to take the values 126, 172, and 184 and the corresponding values of N_{c2} are taken to be 216, 216, and 238. The parameter α_n is increased, only for the case of neutrons, to 6 (6.5) MeV for odd (even) neutron numbers N_n. This modification of the parameters of the

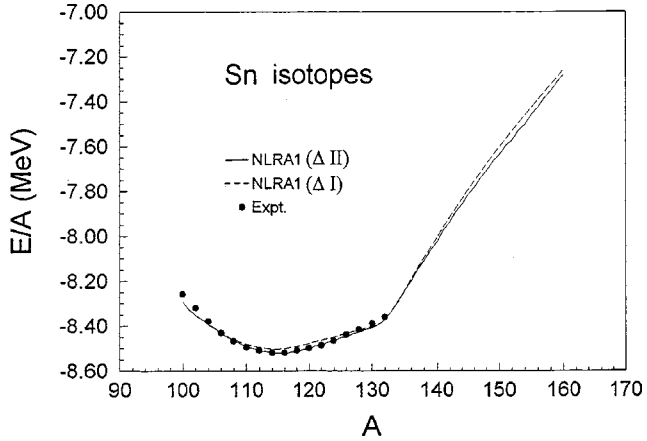

FIG. 2. The binding energy per particle for Sn isotopes, E/A, against mass number A calculated by NL-RA1 force and using model II (solid) and model I (dashed) for pairing.

pairing model II are only considered for superheavy elements that will be discussed in detail in Secs. V and VI.

IV. EXOTIC NUCLEI

In this section we are interested with exotic nuclei in the heavy region, such as Sn and Pb isotopes. The Sn isotopes are of particular interest for nuclear structure and also astrophysical questions because of the closure of the $Z=50$ proton shell. The known isotopes cover the range from the proton dripline at ^{100}Sn to the doubly magic ^{132}Sn nucleus which is already β unstable. Here, we are mainly interested in investigating the isotopic properties of the relativistic effective interaction NL-RA1, and as a more general aspect, to test relativistic interactions, determined from symmetric nuclear matter and stable nuclei in regions far off stability.

Relativistic mean-field calculations employing the NL-RA1 force and experimental binding energies are compare in Figs. 2 and 3 for Sn and Pb isotopes. The separation energies for Sn isotopes are shown in Fig. 4. As shown from these figures the NL-RA1 force gives a fair description of the experimental binding for both Sn and Pb isotopes, especially with model II pairing. Figures 2 and 3 also show that around

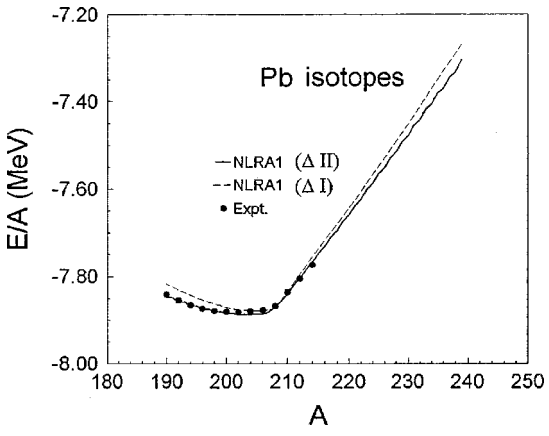

FIG. 3. The same as Fig. 2 but for Pb isotopes.

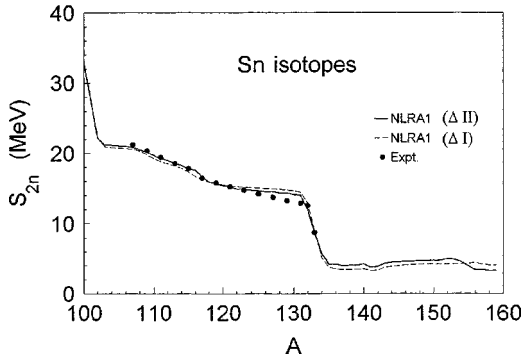

FIG. 4. The two neutron separation energies of Sn isotopes.

^{50}Sn, ^{132}Sn, and ^{208}Pb the binding energies calculated by models Δ I and Δ II are close together, since nuclei at these regions are almost spherical. The strongest binding is obtained for the case of Sn isotopes, at ^{116}Sn, consistent with experiments. The experimental minimum of ^{208}Pb isotopes is also reproduced, as shown from Fig. 3. At the magic shells a strong sudden decrease is observed in the two-neutron separation energy, as expected (see Fig. 4). The magic jump in the two-nucleon separation energy

$$S_{2n}(N,Z)=E(N-2,Z)-E(N,Z),$$

$$S_{2p}(N,Z)=E(N,Z-2)-E(N,Z) \tag{18}$$

is of quite some interest since it can be used for measuring shell closures in the superheavy element, as will be discussed in Sec. VI.

In comparison with the other relativistic forces we found that the NL-SH and TM1 forces predict a relatively larger binding for Sn and Pb isotopes. The results for Pb isotopes calculated using NL-SH, TM1, and NL1 are shown in Figs. 5, 6, and 7, respectively. The NL1 force shows a systematic deviation, where it predicts a larger binging for isotopes lighter than ^{212}Pb, while it predicts a much smaller binding, where the binding energy decreases more and more with increasing neutron numbers, for isotopes heavier than ^{212}Pb, as shown from Fig. 7. This great discrepancy of NL1 is inevitably due to the large asymmetry energy predicted by this

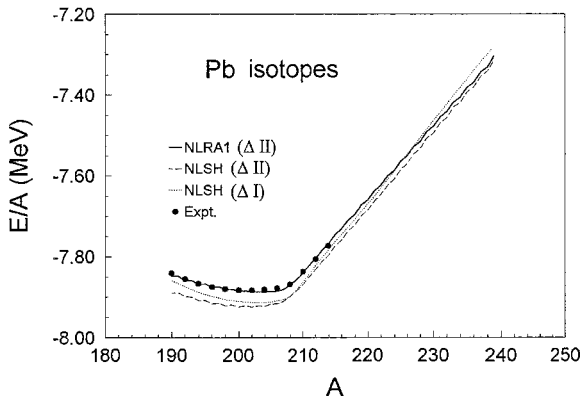

FIG. 5. A comparison between NL-RA1 (see Fig. 2) and NL-SH for the binding energies of Pb isotopes.

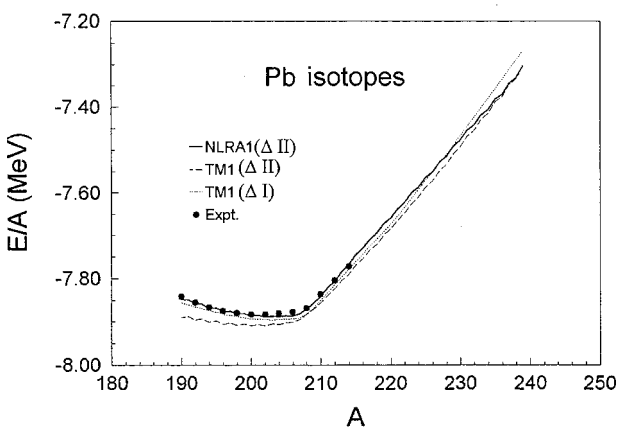

FIG. 6. The same as Fig. 5 but for TM1 force.

force. The NL-SH and TM1 forces predict slightly larger binding, especially for isotopes around and lighter than ^{208}Pb.

Neutron density distributions for several Sn and Pb isotopes are displayed in Figs. 8 and 9, calculated by NL-RA1, using model II for pairing. Figures 10 and 11 display proton and neutron rms radii for Sn and Pb isotopes. The neutron densities show a more drastic evolution. For Sn isotopes, beyond ^{132}Sn an extremely thick neutron skin builds up, leading to a sudden jump in the neutron rms radii. The neutron skin thickness is more clearly visible in Fig. 12 for Sn isotopes, where the difference of the proton and neutron rms radii is shown. The densities of Pb isotopes also show a thick neutron skin is building up for isotopes beyond ^{208}Pb. The saturation of the rms values around $A=132$ in the case of Sn isotopes and around $A=208$ in the case of Pb isotopes are an indication of the double magic nature of ^{132}Sn and ^{208}Pb. The increase is directly related to the shell structure in the heavy isotopes. For example, in the case of Sn isotopes, at $A=132$ the $1h_{11/2}$ shell is filled and pairing does not contribute. At larger masses the neutron $3p$ subshells become populated. Weak binding and the low angular barrier allow a large extension of valence wave functions into the exterior, thus causing this extremely thick neutron skin.

A quite interesting observation is made from Fig. 12 on the neutron-poor side. At the neutron-rich side the excess

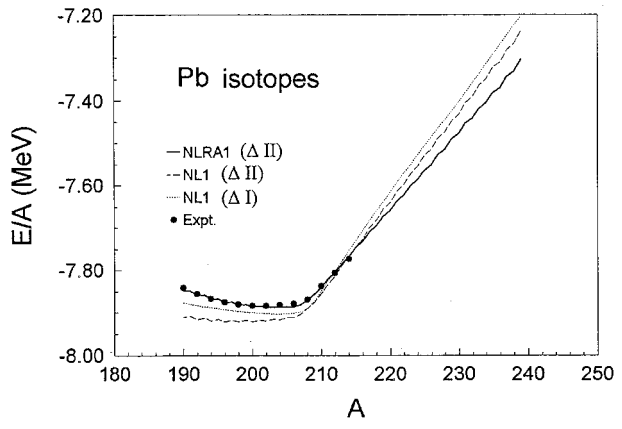

FIG. 7. The same as Fig. 5 but for NL1 force.

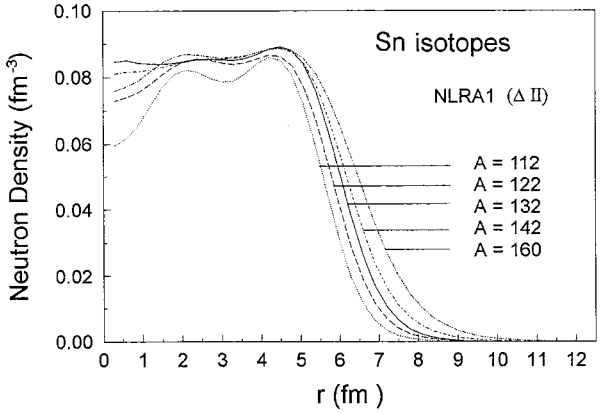

FIG. 8. Neutron density distributions of several Sn isotopes ranging from $A=112$ to 160, calculated by the NL-RA1 force and using model II of pairing.

neutrons become less bound because of increasing repulsion from the isovector potential. Since p states and states with larger angular momentum are involved they are stored predominantly in the surface and tail region in the nucleus. In heavy isotopes the isovector interaction acts attractively in the proton sector and thus balances to a large extent the Coulomb repulsion. Since for nuclei with neutron and proton numbers close together the isovector part of the mean-field becomes strongly suppressed the repulsion is no longer compensated and Coulomb effects become visible. Hence, the proton skin in the neutron-poor Sn nuclides is caused solely by the Coulomb interaction.

Finally, we investigate the anomalous behavior of the charge radii of the isotopic chain of Pb isotopes. The charge radii of Pb isotopes and their isotope shifts have been a matter of detailed discussion within the framework of nonrelativistic [57] and relativistic mean fields [39,48]. The isotopic chain of Pb nuclei exhibits a well-known kink in the behavior of the empirical isotope shifts. On the nonrelativistic side, it has been found that most of the old Skyrme forces that can describe the isotope shifts on the lighter side of ^{208}Pb, using a density-dependent pairing, cannot reproduce the isotope shifts of the heavier counterparts [57]. On the relativistic side, the charge radii and isotope shifts of ^{208}Pb have been

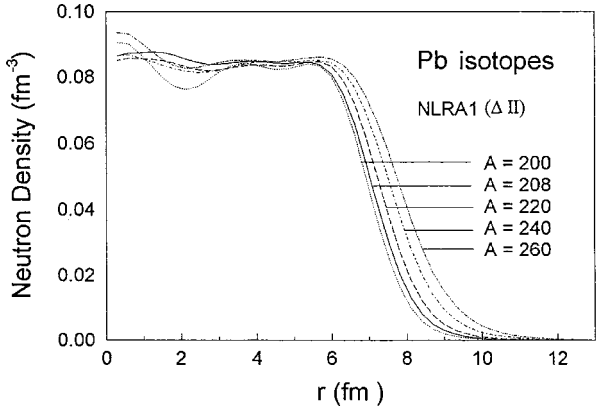

FIG. 9. The same as Fig. 8 but for Pb isotopes ranging from $A=200$ to 260.

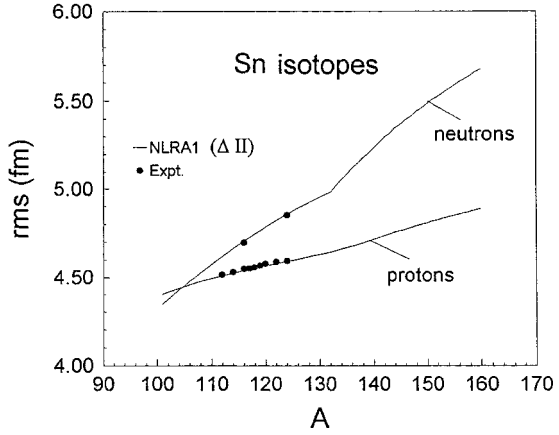

FIG. 10. Neutron and proton rms radii of Sn isotopes, calculated by the NL-RA1 force and using model II for pairing.

approximately reproduced by the relativistic force NL-SH [39]. Reinhard and Flocard [48] show that these different behaviors of the relativistic and nonrelativistic interactions for the isotope shifts are related to the spin-orbit term used in the parametrization, where the nonrelativistic Skyrme parametrization can approximately produce the isotope shifts by modifying the spin-orbit contribution to the nonrelativistic Skyrme energy density functional. In that work the nonrelativistic Skyrme force SkI4 has reproduced the isotope shifts of Pb isotopes near the magic shells. However, more recently, it has been shown, that the Skyrme force SkI4 overestimated the spin-orbit splitting of the protons in ^{208}Pb by 80% [24].

Since most of the Pb isotopes close to ^{208}Pb are almost spherical, it is interesting to study the charge radii and isotope shifts of Pb isotopes within the present spherical configuration, employing the new relativistic effective interaction NL-RA1. Other relativistic forces like TM1, NL-SH, NL1, NL-Z, and NL-Z2 are also employed. Figures 13 and 14 show the charge radii and isotope shifts of Pb isotopes calculated by NL-RA1 in comparison with the experimental data [58]. The isotope shifts are calculated using the method described in [39]. Results for the charge radii calculated by TM1, NL-SH, and NL1 forces are plotted in Fig. 15 and by NL-Z and NL-Z2 in Fig. 16. As shown from these figures

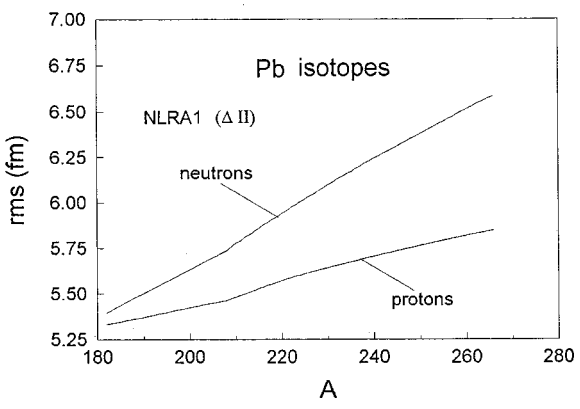

FIG. 11. The same as Fig. 10 but for Pb isotopes.

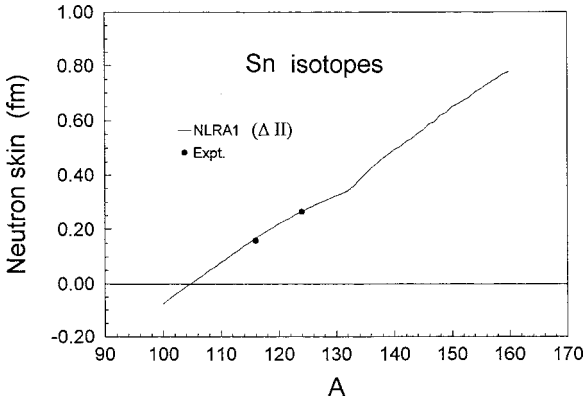

FIG. 12. The same as Fig. 10 but for the neutron skin.

both the charge radii and isotope shifts are fairly reproduced by the relativistic interaction NL-RA1. The TM1 overestimates the charge radii, while the NL-SH predicts smaller radii. The NL-Z and NL-Z2 forces predict much larger charge radii, as shown from Fig. 16. Model II for pairing is found to slightly modify the radii in the lighter side as well as in the heavier counterparts of ^{208}Pb, as shown from Fig. 13. Around ^{208}Pb models II and I for pairing give similar radii, since these nuclei are almost spherical and pairing contributions are negligible.

V. SUPERHEAVY ELEMENTS

Recent years have witnessed great strides in the production of the heaviest nuclei. Notably, three new elements, $Z=110$, 111, and 112, were synthesized at GSI [11–13], Berkeley [14,15], and Dubna [16,17]. More recently evidence of the element $Z=118$ and its α-decay chains may have been observed at Berkeley [18]. These newly developed and the coming experimental facilities produce more new elements and isotopes and the expected magic $Z=114$ seems to be in reach.

In this work we are interested in these new superheavy elements as well as the new isotopes in the region $Z=106$–111. We also investigate the possible existence of

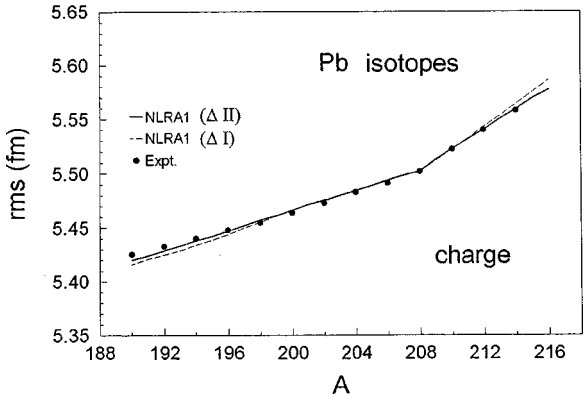

FIG. 13. The charge rms radii of Pb isotopes, calculated by the NL-RA1 force and using models I (dashed) and II (solid) for pairing in comparison with the experimental data.

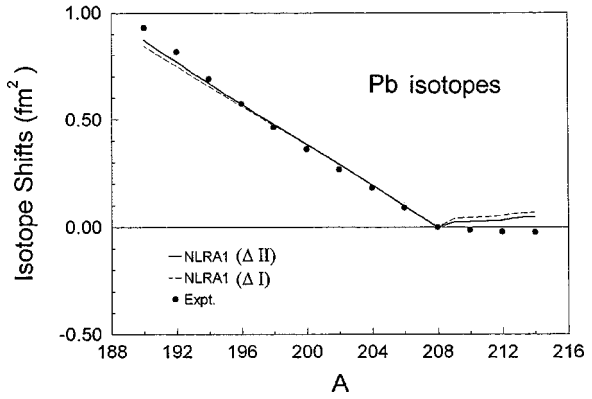

FIG. 14. The same as Fig. 13 but for the isotopic shifts.

spherically doubly magic superheavy nuclei heavier than ^{208}Pb. Theoretical estimates on the basis of the macroscopic-microscopic approaches predicted the element $^{298}_{184}114$ to be the next spherical doubly magic superheavy nucleus to ^{208}Pb [20,21]. On the other hand, most modern parametrization of self-consistent models shifted this property to larger proton and smaller neutron numbers, where the nucleus $^{292}_{172}120$ has been predicted to be the next spherical doubly magic superheavy nucleus [24]. It is thus quite interesting to perform more investigations into superheavy elements within the present microscopic self-consistent model, employing the new relativistic interaction NL-RA1 as well as various relativistic forces. First we test the NL-RA1 force for the binding energy of the known heaviest nuclei. Following [23] we used the heaviest known nuclei starting with $Z=98$ as a benchmark to estimate the predictive value of the forces and models. The most important, and for most superheavy nuclei the only quantitatively known, global ground-state property is the binding energy. The relative error of the binding energy

$$\delta E = \frac{E_{\mathrm{cal}} - E_{\mathrm{expt}}}{E_{\mathrm{expt}}} \tag{19}$$

in percent for the heaviest known nuclei calculated with NL-RA1 force is plotted in Fig. 17. We also calculated δE,

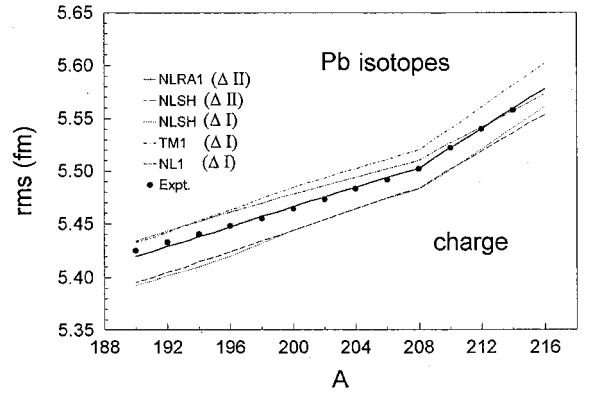

FIG. 15. The same as Fig. 13 in a comparison with NL-SH, TM1, and NL1 forces.

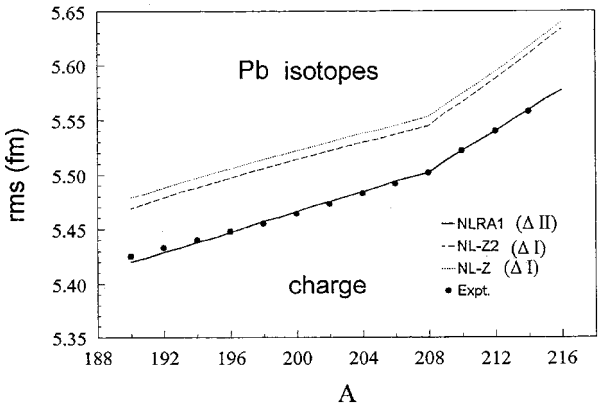

FIG. 16. The same as Fig. 13 in a comparison with NL-Z and NL-Z2 forces.

employing the forces NL-SH, TM1, and NL-Z2 for comparison. Model II of pairing is used in these calculations. As shown from this figure the NL-RA1 force better describes the isotopic trend, where the absolute value of the maximum error is around 0.2%. One also notices that this force predicted reasonable slopes of the errors. The NL-Z2 force predicts a trend similar to the NL-RA1 force, also on the negative side, but with larger errors. The NL-SH and TM1 forces overestimate the binding energy. In [23] the relativistic forces PL-40 and NL3 have been tested and they have been found to predict a wrong isotopic trend, where relatively large positive and negative errors in the slopes have been obtained. Slopes on the negative side have been obtained in [23] only with the nonrelativistic Skyrme forces and the better slopes have been predicted by the Skyrme force SkI4 which, on the other hand, largely overestimates the spin-orbit splitting in ^{208}Pb.

In the next step we calculate the binding energies of the new elements and isotopes in the region $Z=106-111$ [22]. Figure 18 shows the binding energies of the elements ^{256}104, ^{258}105, ^{260}106, ^{262}107, ^{264}108, ^{266}109, ^{269}110, and ^{271}111 calculated by the relativistic force NL-RA1, using model II

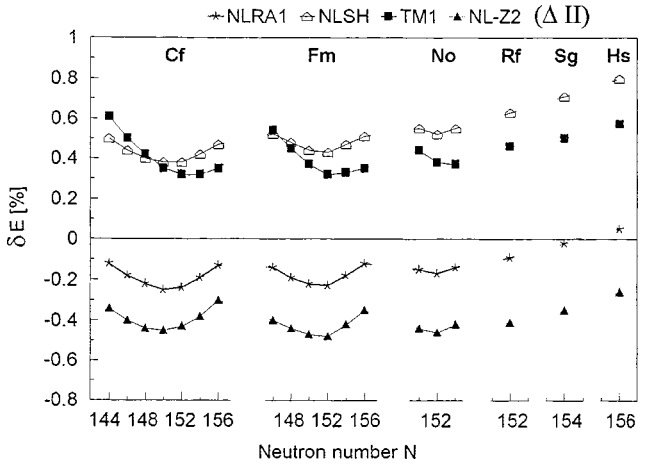

FIG. 17. The relative error in the binding energy in percent for the isotope chains of the heaviest known nuclei, calculated with NL-RA1, NL-SH, TM1, and NL-Z2 forces.

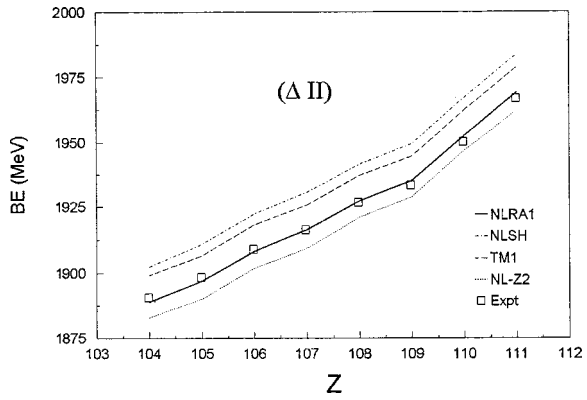

FIG. 18. The negative of the binding energies of the new superheavy elements and isotopes calculated by the NL-RA1 force and using model II for pairing in comparison with NL-SH, TM1, and NL-Z2 forces. The experimental data (bold dots) are taken from [20].

for pairing, in comparison with NL-SH, TM1, and NL-Z2 forces. The experimental data are listed in [20]. As shown from Fig. 18 the NL-RA1 force gives a fair description of the binding energy of all considered superheaviest nuclei. Even the trend of the experimental data, which includes a bend at $Z=109$, are exactly reproduced. The forces NL-SH and TM1 produce larger binding, as in [22], while the NL-Z2 force underbinds the binding energy, as shown in Fig. 18.

VI. THE STRUCTURE OF THE ELEMENT $^{298}_{184}114$

All the heaviest elements found recently are believed to be well deformed. However, spherically doubly magic superheavy elements are still expected, such as the element $^{298}_{184}114$, which was predicted phenomenologically and confirmed recently by macroscopic-microscopic approaches [20,21] to be the next spherical double magic superheavy nucleus. In Fig. 19 we show the proton and neutron single-particle levels of $^{298}_{184}114$ calculated by the relativistic force NL-RA1 in comparison with NL-SH, TM1, and NL-Z2 forces. As indicated from this figure several spherically superheavy nuclei could be predicted at the shell closures $Z=114$, 120, and 138, and at $N=164$, 172, 184, 198, and 228. A small gap at $Z=126$ is predicted by NL-Z2. A quantity, which is important for measuring the magicity, is the two-nucleon energy gap. The two-proton or neutron gap

$$\delta_{2p}(N,Z)=E(N,Z+2)-2E(N,Z)+E(N,Z-2)$$

$$\delta_{2n}(N,Z)=E(N+2,Z)-2E(N,Z)+E(N-2,Z) \quad (20)$$

are related to the two-nucleon separation energies and therefore they can be used to quantify the magicity. At magic shells a pronounced peak can be shown in the two-nucleon gap [23,24]. The two-proton gap δ_{2p} is shown in Fig. 20 for the chain $Z=114$ and in Fig. 21 for the $Z=120$ isotopes. These figures indicate a shell closure at $Z=114$ with a small peak at $N=184$, and at $Z=120$ with a large peak at $N=172$, depending on the effective interaction and pairing model. At the proton shell $Z=114$ the gap is stable. Model II for pairing predicted gaps larger than 3 MeV for all forces, as seen from Fig. 20, which gives strong evidence of the element $^{298}_{184}114$ as being the next doubly magic superheavy element. Although model I of pairing gives smaller gaps, as in

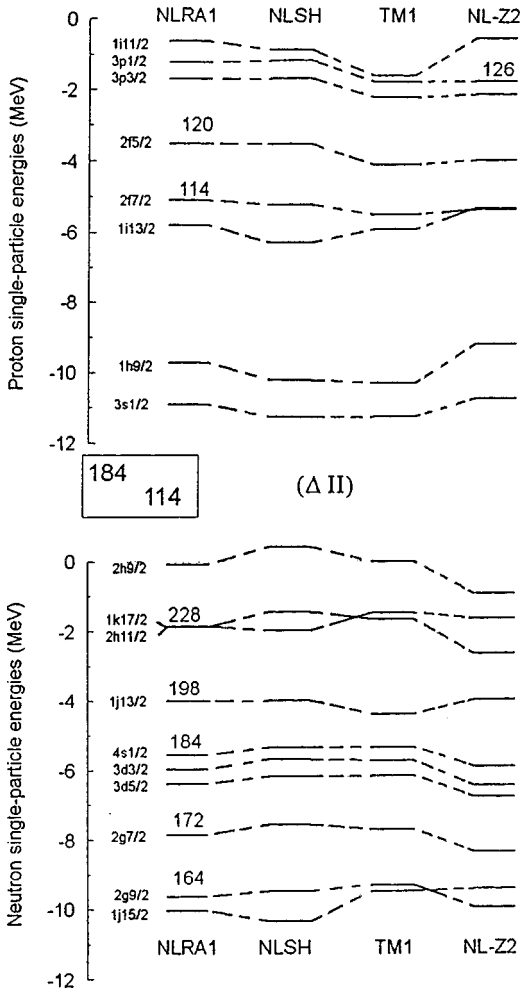

FIG. 19. Single-particle spectra of $^{298}_{184}114$ for protons (top) and neutrons (bottom) in a spherical shape predicted by NL-RA1, NL-SH, TM1, and NL-Z2, and using model II of pairing.

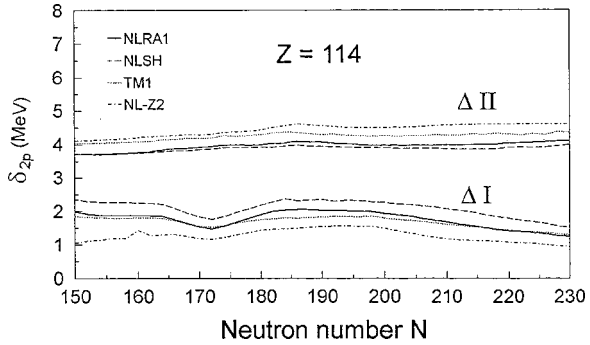

FIG. 20. Two-proton gap in the chain of $Z=114$ isotopes calculated with the relativistic forces NL-RA1, NL-SH, TM1, and NL-Z2, and with models I and II for pairing.

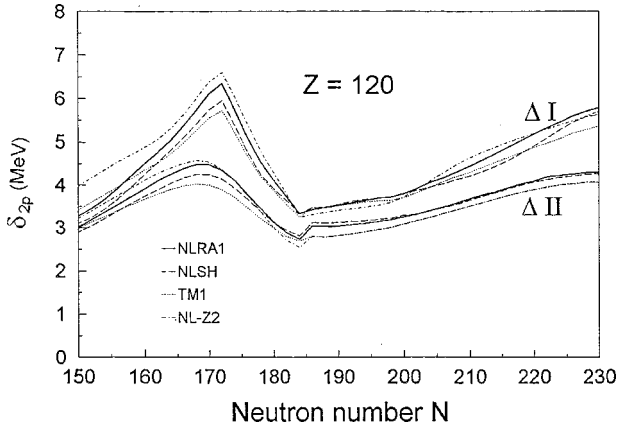

FIG. 21. The same as Fig. 20 but at the proton shell $Z=120$.

[23,24] at the proton shell $Z=114$, the forces NL-RA1 and NL-SH predicted a two-proton gap slightly larger than 2 MeV, at $N=184$, which also indicates the element $^{298}_{184}114$.

The present microscopic self-consistent calculations are consistent with those of the macroscopic-microscopic approaches [20,21]. In comparison with the microscopic nonrelativistic and relativistic calculations of [24] one finds that in [24] the large gap has only been predicted for the element $^{298}_{184}114$ by the Skyrme force SkI4, which largely overestimated the spin-orbit splitting in ^{208}Pb. These different predictions between our work and that of [24] are obviously due to the effective interactions and pairing models. As indicated from the shell structure of the element $^{298}_{184}114$, the possible shell closure at $Z=114$ has been located between two spin-orbit coupled stats: the $2f_{7/2}$ and $2f_{5/2}$ levels. Thus a relatively large spin-orbit splitting is required in order to increase the gap between the two $2f$ states. Additionally the $1i_{13/2}$ state, which has a similar energy to the $2f$ states, has to be pushed down. In this work, most of the relativistic forces (which almost predict a reasonable spin-orbit splitting for finite nuclei) predicted a relatively large spin-orbit splitting between the two $2f$ proton states of $^{298}_{184}114$. Furthermore, the $1i_{13/2}$ state is localized below the $2f$ states, as seen from Fig. 19, which increases the gap at $Z=114$. Furthermore, the pairing model II, which has been found to better describe the binding and separation energies, increases the two-nucleon energy gap at the proton shell $Z=114$ and the neutron shell $N=184$, especially with a better choice of the parameters of this model.

Finally, it is important to note that the element $^{292}_{172}120$ is also predicted in this work to be a spherically doubly magic superheavy nucleus, consistent with [23,24]. This is shown in Fig. 21, where a large pronounced peak is observed for all forces and for models I and II of pairing, at $N=172$ for the chain $Z=120$ isotopes (see also Fig. 19).

VII. SUMMARY AND CONCLUSION

We have carried out a study of exotic nuclei and superheavy elements in the framework of the relativistic mean-field theory, which is very powerful for a microscopic description of nuclear systems. We have introduced a new relativistic force, NL-RA1, which well describes finite nuclei and nuclear matter. Pairing correlations are treated by the BCS formalism by introducing a new model for the energy gap. This model has been found to be important in describing exotic nuclei as well as superheavy elements. Studying of nuclei far from stability and superheavy elements is quite interesting since they provide a good test for effective interactions and models derived from nuclear matter and stable nuclei. The new relativistic NL-RA1 force has been found to give a fair description of Sn and Pb isotopes, where the binding and separation energies, the proton and neutron radii, and the neutron distributions are better described. For Sn isotopes beyond ^{132}Sn and for Pb isotopes beyond ^{208}Pb the neutron densities and rms radii show an extremely thick neutron skin is building up, leading to a sudden jump in the neutron radii. The isotope shifts in ^{208}Pb isotopes and the charge radii are also found to be fairly described by the NL-RA1 force. Different relativistic forces have been tested and they are found to give different predictions. For example, the NL1 force showed great discrepancies, where it neither describes the binding energies of Pb isotopes nor the charge radii well, due to their larger symmetry energy. The TM1 force overestimated the charge radii of Pb isotopes, while the NL-SH predicted smaller radii. The NL-Z and NL-Z2 forces overestimated the radii larger than TM1.

The NL-RA1 force is used to study the well known superheavies in the region $Z\geqslant 98$ and the new superheavy elements and isotopes in the region $Z=106$–111. Both the binding energy and the isotopic trend are better described by NL-RA1, where the maximum error in the binding energy has found to be less than 0.25%. The other relativistic forces present larger errors. We also investigated the possible existence of doubly magic superheavy elements that are heavier than ^{208}Pb. The NL-RA1 as well as most of the relativistic forces, like the NL-SH force, gave strong evidence of the element $^{298}_{184}114$ to be the next spherical doubly magic nucleus, consistent with the predictions of macroscopic-microscopic approaches. Several spherical doubly magic superheavy elements are also predicted such as $^{292}_{172}120$, consistent with the microscopic calculations of Bender *et al.* [24]. However, in [24] the element $^{298}_{184}114$ has only been predicted by the nonrelativistic Skyrme force SkI4 which, on the other hand, overestimates the proton spin-orbit splitting in ^{208}Pb by 80% [24]. The relativistic forces used in this work have been tested for the spin-orbit splitting of finite nuclei and they are found to give a quite good description, within an acceptable error. For example, the spin-orbit splitting for the proton $1g$ level in ^{208}Pb predicted by the forces NL-RA1, NL-SH, TM1, and NL-Z2 are about 4.2, 4.3, 3.4, and 4.1 MeV, respectively. In comparison with the experimental data (4 MeV), the forces NL-RA1, NL-SH, and NL-Z2 overestimate the proton spin-orbit splitting of this level by about 5%, 7.5%, and 2.5%, while the TM1 force underbinds this level by about 15%.

The pairing model used in this work (model II) has been found to better describe the binding and separation energies. A quite interesting result of this model is that it can increase

the two-nucleon gap at the proton shell $Z=114$ (to be on the order of 3.5 MeV, depending on the interaction) as well as the neutron shell $N=184$ (to be on the order 2.5 MeV), which is important for the evidence of the element $^{298}_{184}114$. Thus both the effective interaction as well as pairing correlation are very important and should be treated carefully in order to better describe superheavy elements and nuclei far from stability.

[1] W. Nazarewicz, B. Tanihata, and Van Duppen, Nucl. Phys. News **6**, 17 (1996).
[2] J. Dobaczewski and W. Nazarewicz, Philos. Trans. R. Soc. London, Ser. A **356**, 2007 (1998).
[3] A. Mueller, Nucl. Phys. **A654**, 215c (1999).
[4] I. Tanihata, Nucl. Phys. **A654**, 235c (1999).
[5] S. Mizutori, J. Dobaczewski, G.A. Lalazissis, W. Nazarewicz, and P.-G. Reinhard, nucl-th/9911062.
[6] K. Riisager, A.S. Jensen, and P. Moller, Nucl. Phys. **A548**, 393 (1992).
[7] A. Mueller and B. Sherril, Annu. Rev. Nucl. Part. Sci. **43**, 529 (1993).
[8] K. Riisager, Rev. Mod. Phys. **66**, 1105 (1994).
[9] P.G. Hansen, A.S. Jensen, and B. Jonson, Annu. Rev. Nucl. Part. Phys. **45**, 591 (1995).
[10] I. Tanihata, J. Phys. G **22**, 157 (1996).
[11] S. Hoffmann *et al.*, Z. Phys. A **350**, 277 (1995).
[12] S. Hoffmann *et al.*, Z. Phys. A **350**, 281 (1995).
[13] S. Hoffmann *et al.*, Z. Phys. A **354**, 229 (1996).
[14] A. Ghiorso *et al.*, Nucl. Phys. **A583**, 861c (1995); Phys. Rev. C **51**, R2293 (1995).
[15] Yu.Ts. Oganessian, Nucl. Phys. **A583**, 823 (1995).
[16] Y.A. Lazarev *et al.*, Phys. Rev. Lett. **73**, 624 (1994); **75**, 1903 (1995).
[17] Y.A. Lazarev *et al.*, Phys. Rev. C **54**, 620 (1996).
[18] V. Ninov *et al.*, Phys. Rev. Lett. **83**, 1104 (1999).
[19] G.A. Lalazissis, M.M. Sharma, P. Ring, and Y.K. Gambhir, Nucl. Phys. **A608**, 202 (1996).
[20] P. Moeller, J.R. Nix, W.D. Myers, and J. Swiatecky, At. Data Nucl. Data Tables **59**, 185 (1995); P. Moeller and J.R. Nix, Phys. Rev. C **5**, 1050 (1972); Nucl. Phys. **A229**, 229 (1974); **A361**, 117 (1981); Nucl. Part. Phys. **20**, 1681 (1994); nucl-th/9709016.
[21] S. Cwiok, J. Dobaczewski, P.-H. Heenen, P. Magierski, and W. Nazarewicz, Nucl. Phys. **A611**, 211 (1996).
[22] R. K. Gupta, S. K. Patra, and W. Greiner, Mod. Phys. Lett. A **12**, 1727 (1997).
[23] T. Buervenich, K. Rutz, M. Bender, P.G. Reinhard, J.A. Maruhn, and W. Greiner, Eur. Phys. J. A **3**, 139 (1998).
[24] M. Bender, K. Rutz, M. Bender, P.G. Reinhard, J.A. Maruhn, and W. Greiner, Phys. Rev. C **60**, 034304 (1999).
[25] J. Meng and N. Takigawa, nucl-th/9908040.
[26] B.D. Serot and J.D. Walecka, Adv. Nucl. Phys. **16**, 1 (1986).
[27] P.G. Reinhard, Rep. Prog. Phys. **52**, 439 (1989).
[28] B.D. Serot, Rep. Prog. Phys. **55**, 1855 (1992).
[29] P. Ring, Prog. Part. Nucl. Phys. **37**, 193 (1996).
[30] Y.K. Gambhir, P. Ring, and A. Thimet, Ann. Phys. (N.Y.) **198**, 132 (1990).
[31] G. Audi and A.H. Wapstra, Nucl. Phys. **A565**, 1 (1993).
[32] M. Rufa, P.G. Reinhard, J.A. Maruhn, W. Greiner, and M.R. Strayer, Phys. Rev. C **38**, 390 (1988).
[33] M. Rashdan, Phys. Rev. C **48**, 1323 (1993); Nucl. Phys. **A602**, 502 (1996); Phys. Rev. C **54**, 315 (1996); Int. J. Mod. Phys. E **6**, 151 (1997).
[34] M. Rashdan, Phys. Lett. B **395**, 141 (1997).
[35] M.M. Sharma, M.A. Nagarajan, and P. Ring, Phys. Lett. B **312**, 377 (1993).
[36] P.G. Reinhard, M. Rufa, J. Maruhn, W. Greiner, and J. Friedrich, Z. Phys. A **323**, 13 (1986).
[37] Y. Sugahara and H. Toki, Nucl. Phys. **A579**, 557 (1994).
[38] J.N. Ginocchio, Phys. Rev. Lett. **78**, 436 (1997).
[39] M.M. Sharma, G.A. Lalazissis, and P. Ring, Phys. Lett. B **317**, 9 (1993).
[40] H. Kucharek and P. Ring, Z. Phys. A **339**, 23 (1991).
[41] T. Gonzalez-Llarena, J.L. Egido, G.A. Lalazissis, and P. Ring, Phys. Lett. B **379**, 13 (1996).
[42] W. Poeschl, D. Vretenar, G.A. Lalazissis, and P. Ring, nucl-th/9709027.
[43] G.A. Lalazissis, D. Vretenar, W. Poeschl, and P. Ring, Nucl. Phys. **A632**, 363 (1998).
[44] M. Stoitsov, P. Ring, D. Vretenar, and G.A. Lalazissis, Phys. Rev. C **58**, 2086 (1998).
[45] D. Vretenar, G.A. Lalazissis, and P. Ring, Phys. Rev. Lett. **82**, 4595 (1999).
[46] G.A. Lalazissis, D. Vretenar, P. Ring, M. Stoitsov, and L. Robledo, Phys. Rev. C **60**, 014310 (1999).
[47] K. Rutz, M. Bender, T. Buervenich, T. Schilling, P.G. Reinhard, J.A. Maruhn, and W. Greiner, Phys. Rev. C **56**, 238 (1997).
[48] P.G. Reinhard and H. Flocard, Nucl. Phys. **A584**, 467 (1995).
[49] R. Machleidt, Adv. Nucl. Phys. **19**, 1 (1989).
[50] R. Machleidt and R. Brockman, Workshop on Dirac Approaches to Nuclear Physics, Los Alamos, Report No. LAMPF LA-10438-C, 1985 (unpublished).
[51] H. Muether, M. Prakash, and T.L. Ainsworth, Phys. Lett. B **199**, 469 (1987).
[52] R. Machleidt and R. Brockman, Phys. Lett. **160B**, 364 (1985).
[53] R. Machleidt, Adv. Nucl. Phys. **19**, 189 (1989).
[54] M.M. Sharma *et al.*, Phys. Rev. C **38**, 2562 (1988).
[55] J.F. Berger, M. Girod, and D. Gogny, Nucl. Phys. **A428**, 32 (1984).
[56] A. Bohr and B. R. Mottelson, *Nuclear Structure* (Benjamin, New York, 1969), Vol. I, Chap. 2.
[57] N. Tajima, P. Bonche, H. Flocard, P.-H. Heenen, and M.S. Weiss, Nucl. Phys. **A551**, 434 (1993).
[58] E. W. Otten, in *Nuclear Radii and Moments of Unstable Nuclei*, in Treasties on Heavy-Ion Science, Vol. 7, edited by D. A. Bromley (Plenum, New York, 1988), p. 515.